Nanomed Res J 11(3):282-295, Summer 2026

RESEARCH ARTICLE

A Multifunctional Neuroregenerative Hydrogel Incorporating Imipramine-Loaded Nanoparticles and Human Stem Cells for Enhanced Spinal Cord Repair

Nima Hamoun[1], Somayeh Ebrahimi-Barough[1*], Sadegh Shirian[2,3], Nasrin Lotfibakhshaiesh[1], Mahmoud Azami[1], Rezvan Mostoli[4], Jamshid Hajati[1], Jafar Ai[1,5*]

[1] Department of Tissue Engineering, School of Advanced Technologies in Medicine, Tehran University of Medical Sciences, Tehran, Iran

[2] Department of Pathology, School of Veterinary Medicine, Shahrekord University, Shahrekord, Iran

[3] Shiraz Molecular Pathology Research Center, Dr Daneshbod Path Lab, Shiraz, Iran

[4] Department of Clinical Biochemistry, Faculty of Medicine, Hamedan University of Medical Sciences, Hamedan, Iran

[5] Brain and Spinal Cord Injury Research Center, Neuroscience Institute, Tehran University of Medical Sciences, Tehran, Iran

ARTICLE INFO

Article History:
Received: 2026-04-27
Revised: 2026-07-27
Accepted: 2026-08-05

Keywords:
Neuroactive hydrogel
Imipramine delivery
Chitosan/alginate scaffold
Spinal cord regeneration

ABSTRACT

Objective(s): Achieving functional recovery after spinal cord injury (SCI) remains a major clinical challenge due to limited axonal regeneration and the inhibitory microenvironment at the lesion site. Here, we introduce a multifunctional, neuroactive hydrogel system that integrates controlled drug delivery and stem cell therapy to synergistically promote axonal regeneration. This biomaterial combines a chitosan/alginate (Ch/Alg) hydrogel with imipramine-loaded chitosan nanoparticles (ChNps-Imp) and human endometrial stem cells (EnSCs).

Methods: We engineered a composite Ch/Alg/ChNps-Imp hydrogel scaffold and characterized its structural, mechanical, and drug release properties. Scaffold morphology and hEnSC adhesion were assessed via scanning electron microscopy (SEM), while cell viability and proliferation were quantified using MTT assays. In vivo efficacy was tested in a rat spinal cord hemisection model, with motor recovery monitored via BBB scoring and axonal regeneration assessed histologically.

Results: The hydrogel demonstrated a highly porous structure, favorable mechanical properties, and sustained release of the neuroactive antidepressant imipramine. SEM imaging showed robust stem cell attachment. In vivo, the Ch/Alg/ChNps-Imp + EnSCs construct led to superior axonal preservation, reduced lesion size, and marked improvements in locomotor function.

Conclusions: This study presents a novel integrative strategy for SCI repair, combining drug-releasing nanoparticles, neuroactive signaling, and stem cell therapy within a biocompatible scaffold. The resulting platform offers enhanced neural regeneration and functional restoration, positioning it as a promising candidate for translational spinal cord repair therapies.

How to cite this article
Hamoun N, Ebrahimi-Barough S, Shirian S, Lotfibakhshaiesh N, Azami M, Mostoli R, Hajati1, Jafar Ai J. A Multifunctional Neuroregenerative Hydrogel Incorporating Imipramine-Loaded Nanoparticles and Human Stem Cells for Enhanced Spinal Cord Repair. Nanomed Res J, 2026; 11(3): 282-295. DOI: 10.22034/nmrj.2026.03.008

* Corresponding Author Email: *jafar_ai@tums.ac.ir*
ebrahimi_s@sina.tums.ac.ir

This work is licensed under the Creative Commons Attribution 4.0 International License.
To view a copy of this license, visit http://creativecommons.org/licenses/by/4.0/.

INTRODUCTION

Spinal cord injury (SCI) is a devastating condition that often results in permanent neurological and functional impairments, arising from either traumatic events or underlying diseases[1-3]. SCI disrupts motor and sensory pathways and impairs autonomic function below the injury site, leading to chronic pain and persistent neuropathic symptoms[1-4]. The pathophysiological cascade triggered by SCI includes ischemia, oxidative stress, edema, lipid peroxidation, excessive accumulation of neurotransmitters, arachidonic acid release, and an inflammatory response. These factors ultimately contribute to apoptotic cell death and the breakdown of ATP-dependent cellular processes at the lesion site[5]. The central nervous system (CNS) exhibits a limited intrinsic ability to regenerate, primarily due to the formation of an inhibitory microenvironment surrounding the injury site, including glial scarring, axonal growth inhibitors, and a general lack of regenerative cues[4]. To address these challenges, significant advances have been made using cell therapy, delivery of bioactive molecules, and biomaterial-based scaffolds to support axonal regeneration[6,7]. Among cell-based approaches, multipotent stem cells have been transplanted via intravascular infusion, intrathecal injection, or direct intraparenchymal delivery to facilitate tissue repair[8]. Imipramine (Imp), a tricyclic antidepressant, has demonstrated neuroprotective and anti-inflammatory effects and is occasionally employed for treating chronic neuropathic pain. [9] Studies suggest that Imp can modulate the NF-κB signaling pathway, reduce tissue inflammation and edema, and mitigate pathological changes following SCI, including decreased myeloperoxidase (MPO) activity and NF-κB DNA-binding[10-14]. Hydrogels—particularly those derived from natural polysaccharides—have emerged as promising scaffolds in neural tissue engineering due to their biocompatibility, biodegradability, and ability to mimic the extracellular matrix[15,16]. Polysaccharide-based hydrogels can provide a supportive three-dimensional framework to guide axonal regrowth and can be functionalized with neuroactive agents to enhance repair[17-19]. Alginate (Alg), a hydrophilic and negatively charged polysaccharide composed of β-D-mannuronic and α-L-guluronic acid residues, is widely used due to its mild gelation properties, tunable mechanical strength, and favorable cytocompatibility[20-24]. Chitosan (Ch), another naturally derived polysaccharide consisting of N-acetyl-D-glucosamine and D-glucuronic acid units, is well known for its biocompatibility, low immunogenicity, and slow degradation rate[16,25]. As a cationic polymer, Ch can form non-covalent complexes with anionic polymers like alginate, enabling the development of physically crosslinked hydrogels with enhanced properties for drug delivery and tissue repair[26,27]. Endometrial stem cells (EnSCs) have shown potential in promoting axonal regeneration and supporting CNS repair[6].

In this study, we developed a neuroactive hydrogel scaffold composed of alginate and chitosan, incorporating imipramine-loaded chitosan nanoparticles. We investigated its biophysical properties and evaluated its suitability for EnSC culture. Following implantation into dorsally hemisected spinal cords of adult rats, we assessed cell viability, axonal regeneration, myelination, and motor function recovery to evaluate the therapeutic efficacy of this multifunctional platform.

MATERIALS AND METHODS

Materials

Chitosan (degree of deacetylation: 84%; weight-average molecular weight: 83 kDa), β-glycerol phosphate, and imipramine hydrochloride (Imp) were obtained from Sigma-Aldrich (USA). Alginic acid (molecular weight ~70 kDa) was supplied by Qingdao Huanghai Biological Pharmaceutical Co., Ltd. (Qingdao, China). Acetic acid was procured from Merck (Germany), and all other reagents were of analytical grade and sourced from commercial suppliers. Prior to hydrogel preparation, the polymers and imipramine were sterilized by rinsing with 70% ethanol and subsequently dried under vacuum. Aqueous solutions of these components were prepared under sterile conditions, following previously reported protocols [28].

Isolation and Culture of Human Endometrial Stem Cells

Human endometrial stem cells (hEnSCs) were isolated following a previously established and validated protocol. [6] Endometrial biopsies were obtained from healthy female donors aged 20–35 years after informed consent and approval by the Ethics Committee of Tehran University of Medical Sciences (Ethical Code: IR.TUMS.VCR.REC.1398.822). The tissues were enzymatically digested with Collagenase A at 37 °C for 45 minutes, and the resulting cell suspension was

CC BY

subjected to Ficoll density gradient centrifugation to isolate mononuclear cells. Cells were cultured in Dulbecco's Modified Eagle Medium (DMEM; Gibco, USA) supplemented with 10% fetal bovine serum (FBS), 100 µg/mL penicillin, and 75 µg/mL streptomycin at 37 °C in a humidified atmosphere of 5% CO_2. Upon reaching ~80% confluency, cells were harvested using trypsin-EDTA and used for subsequent experiments after passage three. The characterization profile of the hEnSCs, including surface marker expression and multilineage differentiation potential, has been reported previously[6].

Imipramine Encapsulation in Chitosan Nanoparticles

Chitosan nanoparticles (ChNPs) loaded with imipramine (Imp) were prepared using the ionic crosslinking and ionotropic gelation method as previously described.[16] Briefly, chitosan was dissolved at 3 mg/mL in acetic acid buffer (pH 4.5), while imipramine hydrochloride was separately dissolved at 1.5 mg/mL in pure acetone. Equal volumes of the two solutions were thoroughly mixed to ensure uniform dispersion.

Additionally, a 1.5 mg/mL imipramine solution prepared in distilled water was added dropwise to the chitosan mixture, maintained at 40 °C. Subsequently, tripolyphosphate (TPP) at 1 mg/mL was added to the chitosan solution (TPP:chitosan volume ratio of 1:6) using a syringe pump at a controlled rate of 25 µL/min under continuous magnetic stirring in 1000 rpm, at 40 °C for 45 minutes to induce nanoparticle formation via ionic crosslinking.

Formed nanoparticles were collected by centrifugation at 14,000 rpm for 30 minutes and washed multiple times with distilled water to eliminate unreacted materials. The purified chitosan nanoparticles were finally freeze-dried using lyophilization for subsequent use.

Hydrogel Preparation

Hydrogels were formulated by dissolving 500 µL of precursor polymer derivatives and imipramine-loaded nanoparticles in Krebs-Ringer-Hepes-bicarbonate (KRH) buffer (pH 7.2). Final concentrations of alginate, chitosan, and nanoparticles in the hydrogel precursor solution were 1.2%, 2.4%, and 0.12% (w/v), respectively. The resulting polymer mixture was combined with beta-glycerol phosphate (2 mg/mL) at a 5:1 volume ratio to initiate gelation.

The mixture was then transferred into a 24-well tissue culture plate and allowed to stand undisturbed at room temperature for 4 hours to ensure complete gelation. Following gelation, 2 mL of KRH buffer was added to each well and the gels were washed three times to remove unreacted components and residual substrates.

Hydrogel characterization

The particle size and zeta potential of chitosan nanoparticles (with and without imipramine) were measured using dynamic light scattering (DLS) with a Zetasizer Nano-ZS (Malvern Instruments, Worcestershire, UK). Samples were diluted in distilled water with a viscosity of 1.0 cP prior to analysis. Imipramine-loaded nanoparticles were separated from the aqueous suspension by centrifugation at 20,000 × g and 14°C for 30 minutes. The supernatant was collected, and the free imipramine content was quantified spectrophotometrically at 248 nm.

Encapsulation efficiency (EE) and loading capacity (LC) were calculated using the following formulas:

$$\%EE = [(Wt-Wf)/Wt] \times 100$$

$$\%LC = [(Wt-Wf)/Wc] \times 100$$

Where Wt is the total amount of imipramine, Wf is the free (unencapsulated) imipramine, and Wc is the weight of the nanoparticles.

Fourier transform infrared spectroscopy (FTIR) analysis was performed using a Nicolet NEXUS 670 spectrometer (Thermo Scientific, Waltham, MA, USA) to evaluate the structural characteristics of native imipramine hydrochloride, chitosan polymer, and imipramine-loaded chitosan nanoparticles. Hydrogel scaffolds, both with and without seeded cells, were rinsed with KRH buffer and fixed in 0.05% glutaraldehyde at 4°C. The samples were then dehydrated through a graded ethanol series (50% to 96%), subjected to critical point drying, and examined by scanning electron microscopy (SEM) using an AIS2100 instrument (Seron Technology, Korea).

he spectra obtained for Imp

hydrochloride, polymers, and physical mixtures of Imp

hydrochloride with polymers were compared

he spectra obtained for Imp

hydrochloride, polymers, and physical mixtures of imipramine

hydrochloride with polymers were compared

(cc) BY

In vitro release study

A specific quantity of imipramine (Imp)-loaded chitosan nanoparticles, both free and encapsulated within hydrogels, were separately suspended in Corning tubes containing tenfold volumes of Krebs-Ringer-Hepes-bicarbonate (KRH) solution (pH 7.2). The tubes were incubated at 37°C with shaking at 100 rpm. At predetermined time points (1, 6, 12, 24, 48, 72, 96, 120, 144, and 168 hours), one tube was retrieved and centrifuged at 20,000 × g for 30 minutes. The concentration of released imipramine in the supernatant was quantified by measuring absorbance at 248 nm using spectrophotometry.

Biocompatibility of hydrogel

The cytocompatibility of the hydrogel was evaluated by assessing the proliferation of human endometrial stem cells (EnSCs) seeded onto the hydrogel scaffold. Briefly, 3 × 10^5 EnSCs were suspended in 500 µL of precursor hydrogel solution containing 0.1% (w/v) chitosan nanoparticles loaded with imipramine and seeded into each well of a 24-well plate. Subsequently, 100 µL of beta-glycerolphosphate was added to initiate hydrogel formation. Following a 4-hour incubation at room temperature to allow gel formation, the scaffolds were rinsed with Krebs-Ringer-Hepes-bicarbonate (KRH) buffer, and 2 mL of culture medium supplemented with 10% fetal bovine serum (FBS) was added to each well. The constructs were then incubated for extended culture periods. Cell morphology on the scaffold was examined using scanning electron microscopy (SEM). Cell proliferation was quantitatively assessed by the MTT assay, measuring formazan salt formation according to the manufacturer's instructions. After 1, 3, and 5 days of culture, MTT reagent (0.5 mg/mL) was added and incubated for 4 hours at 37 °C. The medium was then carefully removed, and the hydrogels were rinsed twice with PBS. To dissolve the formazan crystals produced by viable cells, 500 µL of DMSO was added to each well. The plates were incubated for 4 hours at 37 °C under gentle shaking to ensure complete diffusion. Importantly, after complete extraction, the DMSO–formazan supernatant was carefully transferred to a new 96-well plate, and the optical density (OD) was measured at 570 nm using a microplate reader.

The uniform penetration of MTT within the hydrogel was verified by observing homogeneous purple coloration throughout the constructs, indicating effective diffusion and metabolic reduction of MTT within the 3D matrix. Optical density values were obtained from triplicate samples for each group. Prior to hydrogel preparation, all substrates and reagents were sterilized using a two-step procedure. First, materials were rinsed with 70% ethanol for surface decontamination and allowed to fully evaporate under vacuum. Second, the components were exposed to UV irradiation for 30 minutes on each side. Because UV penetration is limited to a few millimeters, the substrates were spread in a thin layer (<3 mm) to ensure effective sterilization of all surfaces.

In vivo study

Twenty-five adult male Wistar rats, weighing between 200–250 g, were used for surgical procedures. Animals were housed under controlled environmental conditions (22 ± 2 °C, 55 ± 10% humidity, and a 12 h light/dark cycle) with ad libitum access to food and water.

All animal care, handling, and surgical interventions were conducted in accordance with the ethical guidelines of Tehran University of Medical Sciences (Approval Code: IR.TUMS.AEC.REC.1398.822).

Rats were anesthetized by intraperitoneal injection of ketamine (85 mg/kg) and xylazine (15 mg/kg). After shaving and disinfecting the dorsal area with betadine, a midline incision was made to perform a T9–T11 laminectomy. The exposed dura mater was incised and retracted laterally, followed by a dorsal hemisection injury at the T9–T11 spinal levels.[2]

Preparation and Implantation of EnSC-Seeded Hydrogels

Sterilized Ch/Alg and Ch/Alg/ChNps/Imp hydrogels were pre-equilibrated in culture medium overnight. Human endometrial stem cells (EnSCs) were then suspended in Dulbecco's Modified Eagle Medium (DMEM) at a density of 1×10^6 cells/mL and gently mixed with the hydrogel using a wide-bore pipette to ensure even cell distribution. The resulting cell-laden hydrogel was maintained at 37 °C and 5% CO_2 for 30 minutes to promote cell attachment before in vivo implantation.

The animals were randomly assigned into five groups (n=5 per group):

(a) Sham-operated group: laminectomy without SCI (sham)

(b) SCI without treatment (SCI)

(c) SCI treated with chitosan nanoparticles loaded

CC BY

Table 1. Primers for quantitative real-time PCR

Gene	Sequence	Tm (˚C)
Nestin	F: TCAAGATGTCCCTCAGCCTGGA R: AAGCTGAGGGAAGTCTTGGAGC	59
NF	F:CCAAGACCTCCTCAACGTGAAG R:ATGCTTCCCACGCTGGTGAAAC	59
Tuj1	F:GGCCTTTGGACATCTCTTCA R:ATACTCCTCACGCACCTTGC	60
Olig2	F:ATGCACGACCTCAACATCGCCA R:ACCAGTCGCTTCATCTCCTCCA	59
18srRNA	F: GTAACCCGTTGAACCCCATT R: CCATCCAATCGGTAGTAGCG	59

with imipramine, without cells (ChNps/Imp)
(d) SCI treated with chitosan/ alginate hydrogel containing ChNps/ Imp, without cells (Ch/Alg/ChNps/Imp)
(e) SCI treated with Ch/Alg/ChNps/Imp hydrogel seeded with human endometrial stem cells (Ch/ Alg/ChNps/Imp+EnSCs).

The hydrogel scaffolds—with or without EnSCs—were carefully implanted into the spinal cord lesion cavity, which measured approximately 2–3 mm in rostrocaudal length and 1–1.5 mm in depth following the T9–T11 dorsal hemisection. The hydrogel was gently positioned to completely fill the defect without exerting pressure on the surrounding intact neural tissue. After confirming stable placement, the paraspinal muscles were repositioned, and the muscle and skin layers were closed using absorbable vicryl sutures.

Hind limb Motor Function

Motor function of the hind limbs was assessed weekly for four weeks post-injury using the Basso, Beattie, and Bresnahan (BBB) open-field locomotor scale. This scale ranges from 0 (complete paralysis) to 21 (normal locomotion). Two independent observers, blinded to the treatment groups, scored each rat. The BBB scores from both hind limbs were averaged to generate a single score per animal, and group means were calculated.

Tissue Fixation and Histological Preparation

At the end of the 4-week study, animals were euthanized by deep anesthesia with pentobarbital (50 mg/kg, IP). Transcardial perfusion was performed using 100 mL of ice-cold phosphate-buffered saline (PBS), followed by 100 mL of 4% paraformaldehyde (PFA). Spinal cords were dissected, post-fixed in 4% PFA at 4 °C, and processed for paraffin embedding.

Serial longitudinal and transverse sections (5 µm thick) encompassing the lesion site were cut using a microtome and mounted on glass slides. Sections were stained with hematoxylin and eosin (H&E) for general histological assessment of tissue regeneration and inflammation.

RNA Extraction and Quantitative PCR

Total RNA was isolated from spinal cord tissue using the QIAamp RNA Blood Mini Kit (QIAGEN, Cat no. 52304). RNA concentration and purity were measured with a Nanodrop spectrophotometer (BioTek, USA). Complementary DNA (cDNA) synthesis was performed using the Viva 2-step RT-PCR Kit (Cat no. RTPL12).

Gene expression of NF, Nestin, Tuj-1, and Oligo2 was quantified by real-time PCR using CinnaGreen qPCR Mix, 2X (Cat No. MM2041). 18S rRNA served as the endogenous control. The PCR protocol included an initial denaturation at 95°C for 5 minutes, followed by 40 cycles of 95°C for 15 seconds, 56°C for 1 minute, and a melting curve analysis (95°C for 15 seconds, 60°C for 1 minute, 95°C for 15 seconds). Primer sequences are provided in Table 1. Relative expression levels were calculated using the ΔCt method with StepOne software V2.0.

Statistical analysis

Data analysis was performed using SPSS software (Version 22.0, SPSS Inc., Chicago, USA). One-way ANOVA followed by Tukey's post hoc test was used to assess differences among groups. A p-value < 0.05 was considered statistically significant.

RESULTS

Physicochemical characterization nanoparticle and hydrogel

Figure 1 illustrates the overall experimental

(cc) BY

design of the study, including nanoparticle preparation, hydrogel fabrication, in vitro characterization, and in vivo spinal cord injury (SCI) implantation.

The FTIR spectra of the scaffolds are presented in **Figure 2**. The spectra for chitosan (Ch) nanoparticles and imipramine (Imp)-loaded Ch nanoparticles showed characteristic broad -OH stretching and amide (-N-H) bands between 3600–3150 cm^{-1}. The intensity of the amide peak corresponds to partial N-deacetylation of chitin. Distinct absorption peaks were observed at 1637 cm^{-1} (N-H stretching vibration of amine I), 1558 cm^{-1} (amide II carbonyl stretch), and 1414 cm^{-1} (amide III). Additionally, the broad band observed from 1540 to 1647 cm^{-1}—arising from overlapping amide bands of chitosan and carboxyl anions of alginate—confirms the electrostatic interaction between alginate and Ch. The effect of varying Ch concentrations (1, 3, and 5 mg/mL) at a constant TPP concentration (1 mg/mL) on nanoparticle formation and encapsulation efficiency (EE) was evaluated using dynamic light scattering (DLS, Zetasizer). All three concentrations yielded nanoparticles with acceptable polydispersity index (PDI), although aggregate formation with larger diameters was observed at 5 mg/mL Ch. As the Ch concentration increased, both nanoparticle size and PDI increased (230, 260, and 350 nm for 1, 3, and 5 mg/mL Ch, respectively), while EE decreased (64%, 61%, and 44%).

The reduced EE at higher Ch concentrations could be attributed to the amphiphilic nature of Imp, which limits its encapsulation, especially as the Ch/TPP mass ratio increases. This observation is consistent with previous studies reporting that lower Ch/TPP ratios lead to higher EE and improved release profiles. [16] Similarly, the loading capacity (LC) decreased with increasing Ch concentration (45%, 18%, and 9% for 1, 3, and 5 mg/mL Ch, respectively), possibly due to weaker dispersion forces between the amphiphilic Imp and the polymeric matrix. Additionally, lower viscosity in the gelation medium at lower Ch concentrations may facilitate smaller nanoparticle formation, reduce resistance to diffusion in the liquid phase, and enhance EE.

The surface morphology of the hydrogels and nanoparticles was examined by scanning electron microscopy (SEM). **Figure 3** shows porous hydrogel structures with a network of interconnected pores forming a partially uniform, honeycomb-like architecture. Incorporation of nanoparticles did not significantly alter the pore distribution or size. The observed pore diameters ranged from 100 to 200 μm, which is favorable for cell migration and tissue integration.

In vitro release of imipramine

The release profile of imipramine (Imp) from

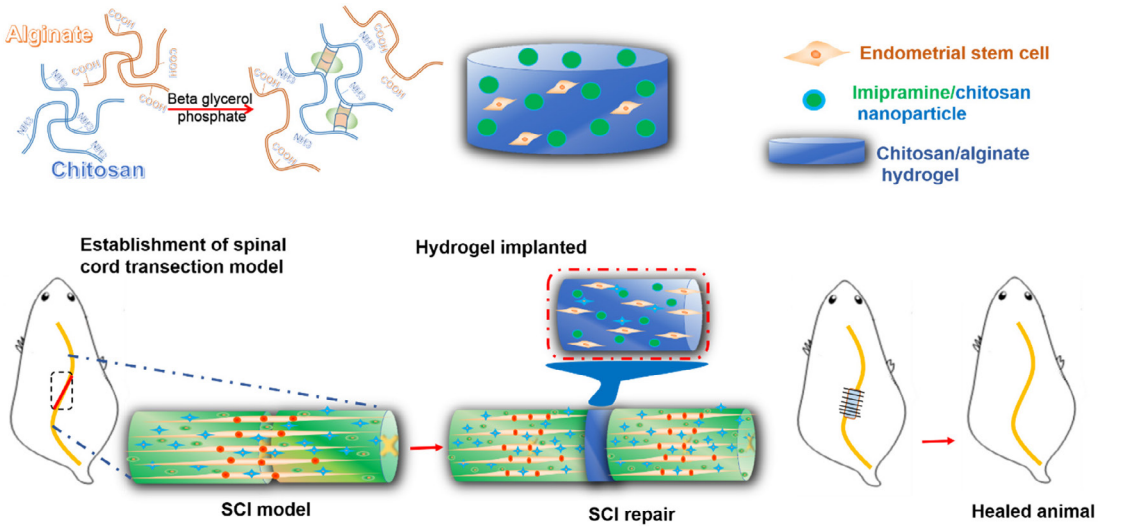


Fig. 1. Schematic representation of the hybrid hydrogel animal experiment, A mixed solution of chitosan and alginate containing Imp loaded chitosan nanoparticle cross-linked through beta glycerol phosphate utilized in regeneration of spinal cord in rat model. After generating the complete transection mouse SCI model, the scaffold was transplanted into the injury site. SCI = spinal cord injury.

CC BY

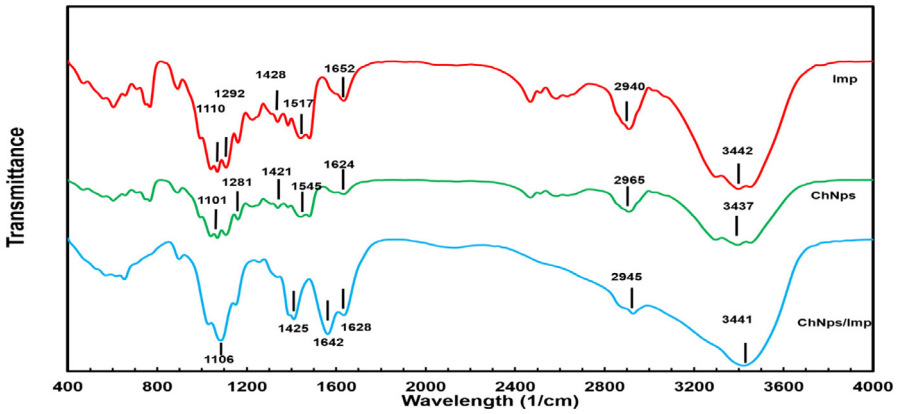


Fig. 2. FTIR spectra of scaffolds: imipramine loaded Ch nanoparticle and Ch nanoparticle and imipramine. FTIR resolution: 4 cm^{-1}.

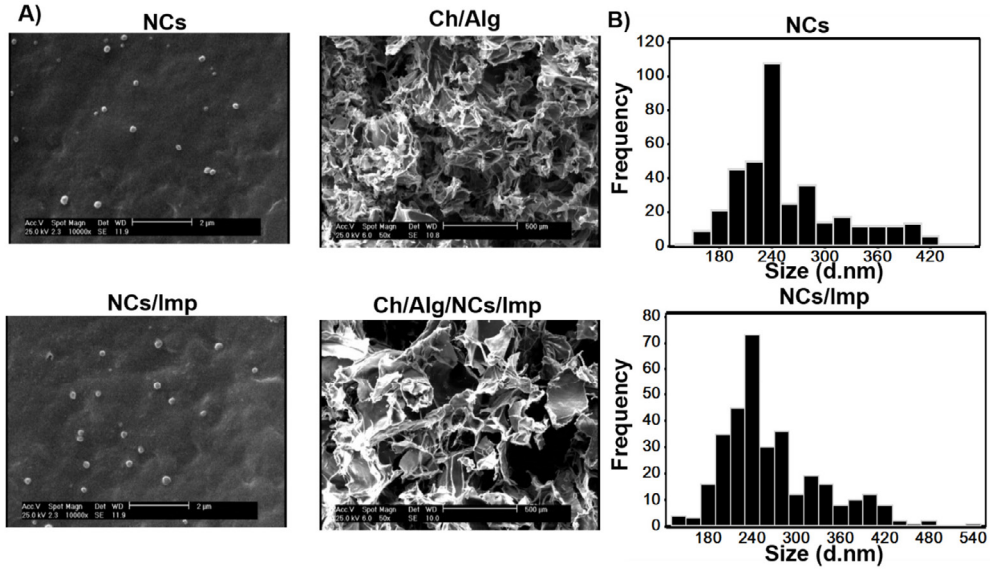


Fig. 3. Scaffold characterization. (A) Field emission scanning Electron micrographs of the synthesized substrates including ChNps, ChNps/Imp, Ch/Algand Ch/Alg/ChNps/Imp. (B) Nanoparticle size distribution without and with imipramine. ChNp: chitosan nanoparticle, NCs/Imp: chitosan nanoparticle loaded with imipramine, Ch/Alg: chitosan/alginate and Ch/Alg/ChNps/Imp: chitosan/alginate containing imipramine-loaded chitosan nanoparticle

the nanoparticle and hydrogel formulations was monitored over 168 hours in phosphate-buffered saline (PBS). As shown in **Figure 4**, the Imp-loaded nanoparticles exhibited an initial burst release of approximately 50% within the first 12 hours, followed by a sustained release phase during which an additional 30% of the drug was released over the next 60 hours. This biphasic pattern is characteristic of nanoparticle systems and can be attributed to the rapid dissociation of loosely adsorbed Imp molecules on the nanoparticle surface, followed by the slower diffusion of entrapped drug from the core.

In comparison, the hybrid Ch/Alg/NCs/Imp hydrogel showed a more controlled and moderate release profile extending over the full 168-hour period. This sustained release behavior is likely due to the physical entrapment of nanoparticles within the hydrogel matrix, which acts as a diffusion barrier, further regulating the drug release rate and minimizing the initial burst. The observed release kinetics suggest that the hybrid system can provide prolonged therapeutic levels of Imp, potentially enhancing its neuroregenerative efficacy.

SEM and Cell proliferation

Scanning electron microscopy (SEM) revealed

(cc) BY

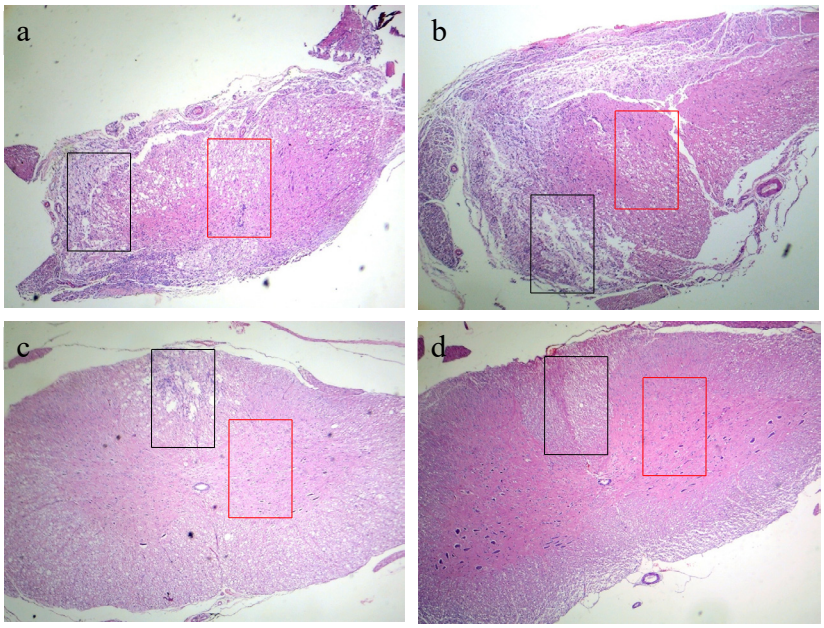


Fig. 4. Release profile of imipramine from ChNps and incorporated into the composite hydrogel after immersion in PBS for different times. (▲)ChNps/Imp and(▪) Ch/Alg/ChNps/Imp. Vertical bars: SDS (n = 4).

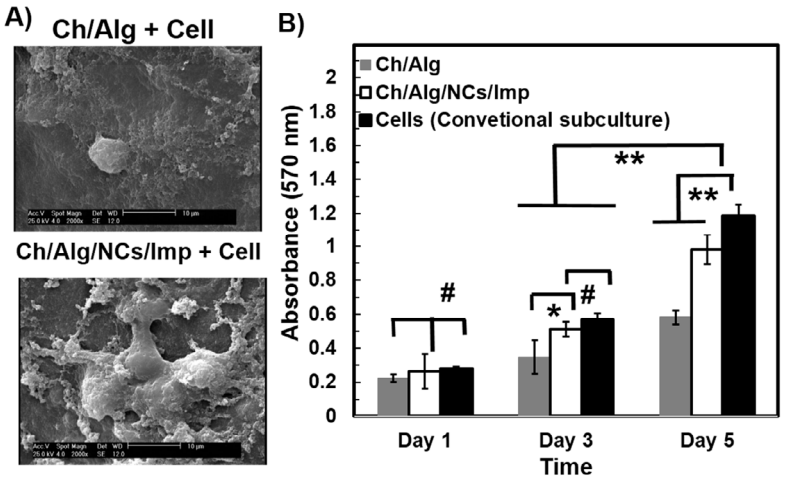


Fig. 5. (A) SEM microphotographs of cell-loaded in hydrogels, (B) Cell viability measurement using MTT assay, The MTT results of EnSCs on cell culture plate, in Ch/Alg and Ch/Alg/ChNps/Imp hydrogels after 1, 3, and 5 days of culture. SD, n =4 (**P< 0.01, *P< 0.05, and $^{\#}P>0.05$).

that human endometrial stem cells (EnSCs) successfully adhered to the surface of all tested hydrogels. Notably, cells seeded on Ch/Alg hydrogels containing Imp-loaded chitosan nanoparticles (ChNps) demonstrated improved attachment and more extensive spreading compared to those on Ch/Alg hydrogels without nanoparticles, where cells predominantly retained a spheroidal morphology with limited surface interaction. In contrast, in the Ch/Alg/ChNps/Imp hydrogel condition, cells exhibited a well-spread morphology and formed more robust cell–material interactions, indicating enhanced biocompatibility and cell support.

Cell viability and proliferation were further quantified using the MTT assay **(Fig. 5).** No statistically significant difference in cell proliferation was observed among Ch/Alg/ChNps/Imp, Ch/Alg, and conventional tissue culture polystyrene (TCP) groups during the first three days of culture (P > 0.05). However, by day 5, the

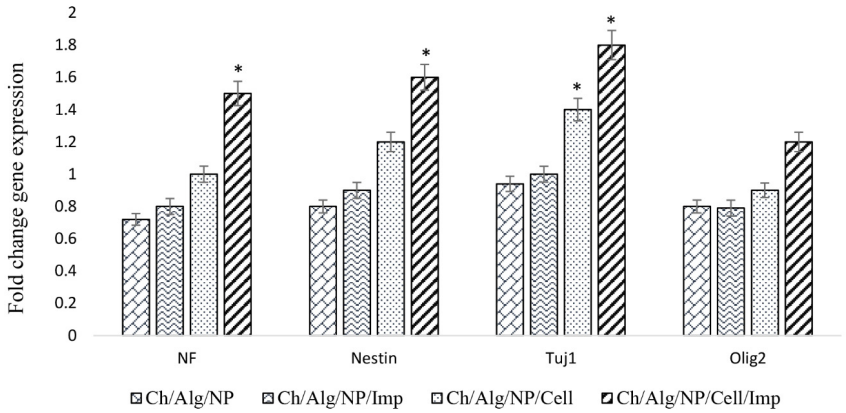


Fig. 6. Gene expression of neuronal and glial markers in different treatment groups following spinal cord injury. Relative mRNA expression levels of NF, Nestin, Tuj1, and Olig2 were quantified by qPCR in animals treated with different hydrogel formulations: Ch/Alg/NP, Ch/Alg/NP/Imp, Ch/Alg/NP/Cell, and Ch/Alg/NP/Cell/Imp. Data are presented as fold change relative to the untreated spinal cord injury (SCI) control group. Asterisks (*) indicate statistically significant differences compared to the control group ($P < 0.05$). Values represent mean ± SD, n = 3 per group.

proliferation rate of EnSCs cultured on Ch/Alg/ChNps/Imp hydrogels significantly surpassed that of the Ch/Alg group ($P < 0.01$), and was comparable to cells cultured on TCP. These results indicate that the Ch/Alg/ChNps/Imp hydrogel scaffold provides a favorable microenvironment for hEnSC adhesion and proliferation, highlighting its potential utility as a cell delivery platform in regenerative medicine applications.

Gene expression analysis

The selected genes (NF, Nestin, TUJ1, and Olig2) represent key markers of neural differentiation and maturation following spinal cord injury. Nestin indicates neural progenitor activation, whereas TUJ1 (βIII-tubulin) and NF reflect neuronal differentiation and axonal regeneration. Olig2 is a transcription factor required for oligodendrocyte lineage specification.

Gene expression analysis revealed significant upregulation of neuronal markers TUJ1, Nestin, and NF in the Ch/Alg/ChNps/Imp/EnSCs group compared with other treatment groups **(Fig. 6).** The Ch/Alg/ChNps/EnSCs group also showed elevated expression of these genes but to a lesser extent. Interestingly, Olig2 expression was significantly downregulated in the Ch/Alg/ChNps/Imp/EnSCs group ($P < 0.05$), suggesting a reduced oligodendrocytic lineage commitment and a potential shift toward neuronal differentiation.

BBB scoring and histological analysis

Locomotor function was evaluated using BBB scoring **(Fig. 7).** Rats treated with Ch/Alg/ChNps/Imp hydrogels exhibited faster and more pronounced functional recovery compared to control and other treatment groups at several time points. Histological analysis revealed severe structural damage to both white and gray matter, with prominent vacuolization and extensive leuko- and poliomyelomalacia in the control group **(Fig. 8A).** In groups treated with ChNps/Imp **(Fig. 8B)** and Ch/Alg/ChNps/Imp **(Fig. 8C),** partial preservation of spinal cord architecture was observed. Notably, the Ch/Alg/ChNps/Imp+EnSCs group **(Fig. 8D)** exhibited improved tissue integrity, reduced vacuolization, and evidence of axonal regeneration, indicating synergistic effects of the stem cell-laden hydrogel in promoting neural repair.

DISCUSSION

In this study, we successfully developed and comprehensively characterized a composite chitosan/alginate (Ch/Alg) hydrogel scaffold embedded with imipramine (Imp)-loaded chitosan nanoparticles (ChNps), and evaluated its potential to promote spinal cord injury (SCI) repair both in vitro and in vivo**.** SCI remains a devastating condition with limited effective treatments, primarily due to the complex secondary injury cascade involving ischemia, oxidative stress, excitotoxicity, and inflammation, which irreversibly impair neural connectivity and function. Our work addresses these challenges by designing a biomimetic scaffold that combines neuroactive drug delivery with stem cell therapy to support

(cc) BY

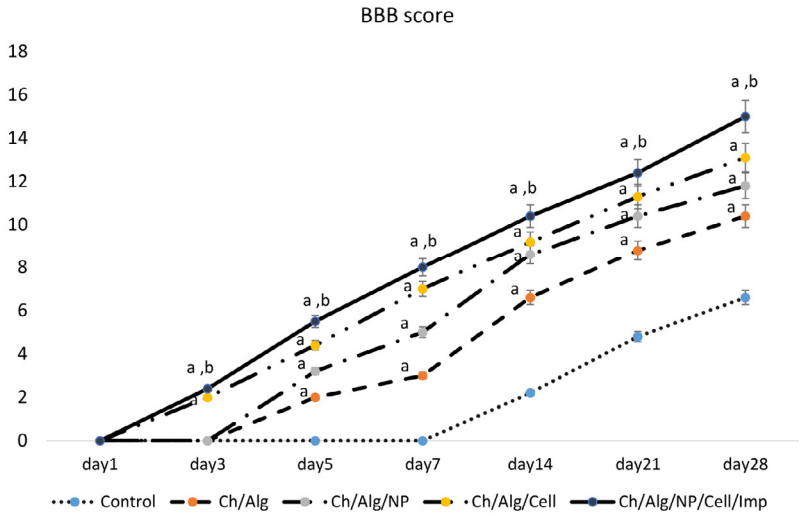


Fig. 7. Basso, Beattie, and Bresnahan (BBB) locomotor scores following treatment. A significant improvement in BBB scores was observed in all treatment groups containing cells—Ch/Alg, Ch/Alg/Np, Ch/Alg/EnSCs, and Ch/Alg/ChNps/Imp—compared to the control group on days 3, 5, 7, 14, and 28 post-treatment. Furthermore, the Ch/Alg/ChNps/Imp + cell group showed significantly higher BBB scores compared to all other treatment groups on days 7, 14, and 28. *a* indicates $P < 0.001$ versus the control group; *b* indicates $P < 0.001$ for Ch/Alg/ChNps/Imp + cells versus all other treatment groups.

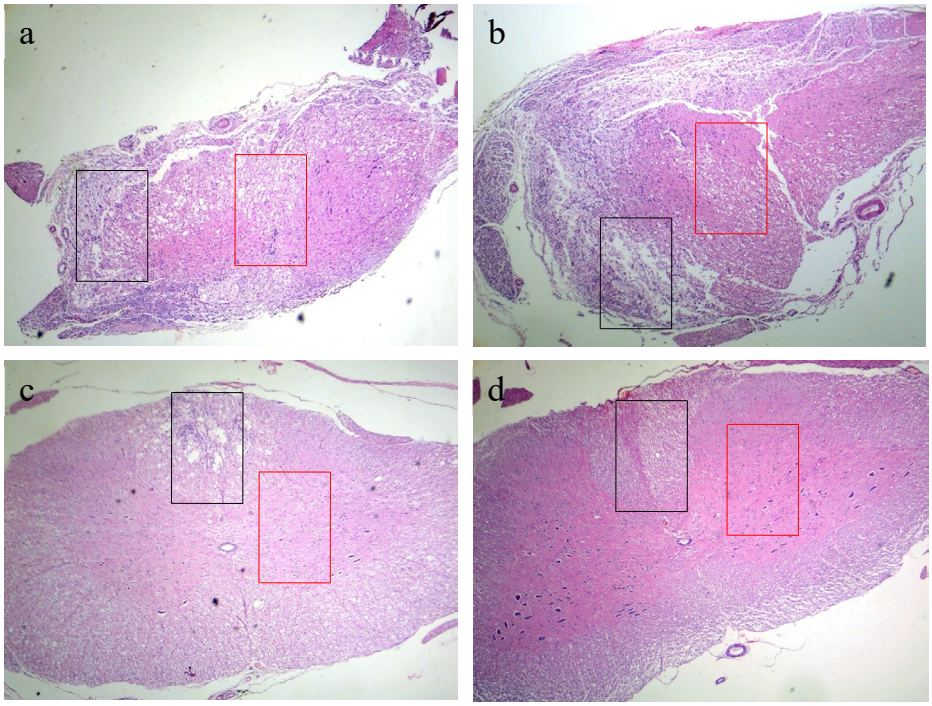


Fig. 8. Histopathological findings in various group, a: the control group or SCI without treatment shows white matters necrosis creating vacuolization spaces indicating sever leukomyelomalacia (black box) as well as gray matter necrosis or poliomyelomalacia (red box) in the control group. b: In the ChNps/Imp group locally extensive white and gray matters necrosis creating vacuolization (red and black boxes) results in disruption of spinal cord structure was seen. c: In the Ch/Alg/ChNps/Imp group partial disruption of spinal cord structure, creating vacuolization spaces indicating gray and white matters polio (red box) and leuko myelomalacia (black box) was detected. d: the Ch/Alg/ChNps/Imp+EnSCs group could improve the disrupted structure of spinal cord and vacuolization spaces and promote the regeneration of the nerve fibers in the white (black box) and gray matters (red box).

axonal regeneration and functional recovery.

The FTIR spectra confirmed successful integration of imipramine-loaded nanoparticles within the Ch/Alg hydrogel, with characteristic amide and carboxyl bands indicating electrostatic interactions between chitosan and alginate polymers. This interaction likely contributes to the structural integrity and stability of the hydrogel network.

The viscosity measurements showed that inclusion of Imp-loaded nanoparticles reduced the Ch/Alg hydrogel's viscosity, likely due to interactions between the functional groups of imipramine and the polysaccharide matrix. This modulation is crucial as it allows tuning of the scaffold's mechanical properties to better match the native spinal cord microenvironment, which is characterized by a delicate balance of stiffness and elasticity. Importantly, the elasticity of the Ch/Alg hydrogel remained below 1000 Pa, an optimal range supporting both neuronal and glial cell survival and proliferation, as previously reported. [29] This mechanical mimicry is vital for cell viability and integration, as excessive stiffness can inhibit neuronal growth and promote glial scarring. The scaffold's porous architecture, confirmed by SEM imaging, displayed an interconnected honeycomb-like microstructure with pore sizes ranging from 100 to 200 μm, ideal for nutrient diffusion, waste removal, and cell migration. SEM also demonstrated that EnSCs seeded on the Ch/Alg/ChNps/Imp scaffold adhered well, spread extensively, and exhibited elongated and branched morphology indicative of active neural differentiation suggesting that the scaffold provides a supportive microenvironment for neural lineage maturation and cell health.

MTT assays reinforced the biocompatibility of the scaffold, showing continuous cell proliferation over five days without cytotoxic effects. In contrast, chitosan-only hydrogels showed less favorable proliferation, likely due to differences in mechanical properties and microenvironmental cues. These results highlight the importance of scaffold composition and drug incorporation for creating a supportive niche for transplanted stem cells.

Molecular analyses revealed significant upregulation of neural markers—Tuj1 (a neuron-specific class III beta-tubulin), Nestin (a neural stem/progenitor marker), and neurofilament (NF, an axonal structural protein)—in the Ch/Alg/ChNps/Imp + EnSCs group compared to controls. This suggests that the combination of the hydrogel scaffold, drug release, and stem cells synergistically promotes neuronal differentiation and axonal maturation. Conversely, the observed downregulation of Olig2, a marker for oligodendrocyte precursor cells, alongside increased markers of mature neurons, indicates that the scaffold encourages maturation of oligodendrocytes rather than maintaining cells in an immature precursor state. This maturation is critical for functional remyelination and restoration of nerve conduction following injury. [30] The controlled release of imipramine likely contributes to this effect, as tricyclic antidepressants have been reported to modulate neurotrophic signaling pathways and enhance neuroregeneration.

Compared with other drug-eluting hydrogels used in spinal cord injury, such as those delivering valproic acid or growth factors (e.g., BDNF, NGF), the imipramine-loaded chitosan/alginate system offers a simpler, more stable, and cost-effective alternative. Imipramine, a small amphiphilic molecule, enables sustained local release without the need for cold-chain preservation required for protein-based systems. The combination of controlled imipramine delivery with a biocompatible Ch/Alg matrix and EnSCs provides synergistic effects through pharmacologic modulation, trophic support, and structural guidance. In contrast, growth-factor-based hydrogels often elicit more potent but less stable biological responses and pose higher immunogenic and manufacturing challenges. While small-molecule systems like ours may produce milder effects, they offer greater formulation stability and translational feasibility. Further optimization of drug loading and release kinetics may enhance efficacy and complement existing growth factor–based strategies. The imipramine release profile from nanoparticles and hydrogel showed an initial burst release (~50% within 12 hours), followed by a sustained release over seven days. This biphasic release is advantageous for SCI therapy, as the initial burst can provide immediate neuroprotective effects by reducing excitotoxicity and inflammation, while the sustained release supports ongoing regeneration and axonal outgrowth. The hydrogel's network efficiently retained the drug-loaded nanoparticles, slowing the release and maintaining local therapeutic concentrations.

In the rat SCI model, implantation of the Ch/

(cc) BY

Alg/ChNps/Imp + EnSCs scaffold significantly improved locomotor function as evidenced by higher BBB scores compared to controls and other treatment groups. Histological analysis confirmed reduced tissue disruption and vacuolization in treated groups, with the hybrid scaffold demonstrating notable preservation of both gray and white matter and increased axonal density at the lesion site. These findings correlate strongly with the improved motor outcomes and suggest that the scaffold promotes both neuroprotection and regeneration. The inclusion of EnSCs within the hydrogel likely contributed to the regenerative effect through paracrine signaling and direct cell replacement, while the controlled release of imipramine enhanced the microenvironment by mitigating secondary injury mechanisms. Together, these factors create a synergistic effect that enhances axonal regrowth, reduces glial scar formation, and supports remyelination.

While our results are promising, the study has limitations. Longer-term assessments are necessary to confirm sustained functional recovery and integration of regenerated axons. Detailed mechanistic studies exploring how imipramine modulates signaling pathways in the SCI microenvironment would deepen understanding. Additionally, optimization of nanoparticle loading and release kinetics could further improve therapeutic efficacy. Future work should also assess immune responses and potential translational aspects in larger animal models.

CONCLUSION

This study successfully fabricated and evaluated a Ch/Alg hydrogel scaffold loaded with imipramine-containing chitosan nanoparticles and human endometrial stem cells for spinal cord injury repair. The scaffold exhibited favorable mechanical and supported cell attachment and proliferation, and provided a conducive environment for neuronal regeneration. Incorporation of Imp-loaded nanoparticles enhanced the scaffold's therapeutic performance without affecting its structural integrity or pore architecture. The composite hydrogel facilitated sustained Imp release, promoted neuronal gene expression, and improved motor function recovery in vivo. These findings underscore the potential of the Ch/Alg/ChNps/Imp+EnSCs hydrogel as a promising biomaterial for SCI treatment and nerve tissue engineering applications.

DATA AVAILABILITY

All source data generated in these studies is available upon reasonable request to the corresponding authors.

CONFLICT OF INTEREST

The authors declare that they have no competing interests.

AUTHORS' CONTRIBUTIONS

Conceptualization: Jafar Ai
Data curation: Nima Hamoun
Formal analysis: Sadegh Shirian
Investigation: Nima Hamoun, Nasrin Lotfibakhshaiesh, Mahmoud Azami, Rezvan Mostoli, Jamshid Hajati
Methodology: Somayeh Ebrahimi-Barough
Project administration: Jafar Ai, Somayeh Ebrahimi-Barough
Resources: Jafar Ai

FUNDING

The authors gratefully acknowledge the support of Tehran University of Medical Sciences (TUMS) and the National Institute for Medical Research Development (NIMAD). This study was funded by TUMS under Grant No. 98-02-87-43326 and by NIMAD under Grant No. 972810. The authors sincerely appreciate the valuable contributions and continued support provided throughout the research.

ACKNOWLEDGMENT

The authors gratefully acknowledge the support of Tehran University of Medical Sciences (TUMS) and the National Institute for Medical Research Development (NIMAD).

ETHICS APPROVAL

The study was approved by the Ethics Committee of Tehran University of Medical Sciences for both human and animal research following approval under the code IR.TUMS.VCR.REC.1398.822, and written informed consent was obtained from all participants. Animal experiments were performed in accordance with the guidelines of the Iranian Ministry of Health and Medical Education as well as international standards for the care and use of laboratory animals.

REFERENCES

1. Zhang H, Xu Q, Wang X, Li Y, Chen L, Liu J, et al. Advances in novel biomaterial-based strategies for spinal cord injury treatment. Mol Pharm. 2024;21(6):2310-2332. https://doi.org/10.1021/acs.molpharmaceut.3c01104
2. Attwell CL, van Zwieten M, Verhaagen J, Mason MRJ. The Dorsal Column Lesion Model of Spinal Cord Injury and Its Use in Deciphering the Neuron-Intrinsic Injury Response. Dev Neurobiol. 2018;78(10):926-951. https://doi.org/10.1002/dneu.22601
3. Fehlings G, Honda S, Vajkoczy P, Nagoshi N. Emerging advances in spinal cord injury: An introductory overview. Brain Spine. 2025;5:104307. https://doi.org/10.1016/j.bas.2025.104307
4. Sugai K, Nakamura M, Okano H, Nagoshi N. Stem cell therapies for spinal cord injury in humans: a review of recent clinical research. Brain Spine. 2025;5:104207. https://doi.org/10.1016/j.bas.2025.104207
5. Hellenbrand DJ, Oakes RS, Sun D, Hagg T. The secondary injury cascade after spinal cord injury: an analysis of local cytokine/chemokine regulation. Neural Regen Res. 2024;19(6):1108-1122. https://doi.org/10.4103/1673-5374.385849
6. Sepehri M, Rabbani S, Ai J, Bahrami N, Ghanbari H, Namini MS, et al. Therapeutic potential of exosomes derived from human endometrial mesenchymal stem cells for heart tissue regeneration after myocardial infarction. Regen Ther. 2025;28:451-461. https://doi.org/10.1016/j.reth.2025.01.007
7. He S, Zhang Z, Zhang L, Chen C, Wang J. Advances in biomaterial-based spinal cord injury repair. Adv Funct Mater. 2022;32(47):22070081. https://doi.org/10.1002/adfm.202110628
8. Lu Y, Wang N, Su L, Zhao W, Wu X, Zhang Y, et al. Stem cell transplantation routes and mechanisms for spinal cord injury repair. Stem Cell Res Ther. 2022;13:441. https://doi.org/10.1186/s13287-022-03103-8
9. Hearn L, Derry S, Phillips T, Moore RA, Wiffen PJ. Imipramine for neuropathic pain in adults. Cochrane Database Syst Rev. 2014;(5):CD010769. https://doi.org/10.1002/14651858.CD010769.pub2
10. Chen S, Ye J, Chen X, et al. Valproic acid attenuates traumatic spinal cord injury-induced inflammation via STAT1 and NF-κB pathway dependent of HDAC3. J Neuroinflammation. 2018;15:150. https://doi.org/10.1186/s12974-018-1193-6
11. Galkina SI, Golenkina EA, Fedorova NV, Ksenofontov AL, Serebryakova MV, Arifulin EA, et al. Inhibition of Neutrophil Secretion Upon Adhesion as a Basis for the Anti-Inflammatory Effect of the Tricyclic Antidepressant Imipramine. Front Pharmacol. 2021;12:709719. https://doi.org/10.3389/fphar.2021.709719
12. Ramirez K, Shea DT, McKim DB, Reader BF, Sheridan JF. Imipramine attenuates neuroinflammatory signaling and reverses stress-induced social avoidance. Brain Behav Immun. 2015;46:212-220. https://doi.org/10.1016/j.bbi.2015.01.016
13. Karol R, Sheridan JF. Antidepressant imipramine diminishes stress-induced inflammation in the periphery and central nervous system and related anxiety- and depressive-like behaviors. Brain Behav Immun. 2016;57:293-303. https://doi.org/10.1016/j.bbi.2016.05.008
14. Yang J, Qu JM, Summah H, Zhang J, Zhu YG, Jiang HN. Protective effects of imipramine in murine endotoxin-induced acute lung injury. Eur J Pharmacol. 2010;638(1-3):128-133. https://doi.org/10.1016/j.ejphar.2010.04.005
15. Afsartala Z, Hadjighassem M, Shirian S, Ebrahimi-Barough S, Gholami L, Parasmanesh G, et al. The Effect of Collagen and Fibrin Hydrogels Encapsulated with Adipose Tissue Mesenchymal Stem Cell-Derived Exosomes for Treatment of Spinal Cord Injury in a Rat Model. Iran J Biotechnol. 2023;21(3):1-13.
16. Chedly J, Soares S, Montembault A, von Boxberg Y, Veron-Ravaille M, Mouffle C, et al. Physical chitosan microhydrogels as scaffolds for spinal cord injury restoration and axon regeneration. Biomaterials. 2017;138:91-107. https://doi.org/10.1016/j.biomaterials.2017.05.024
17. Khanmohammadi M, Dastjerdi MB, Ai A, Ahmadi A, Godarzi A, Rahimi A, et al. Horseradish peroxidase-catalyzed hydrogelation for biomedical applications. Biomater Sci. 2018;6(6):1286-1298. https://doi.org/10.1039/C8BM00056E
18. Boido M, Ghibaudi M, Gentile P, Favaro E, Fusaro R, Tonda-Turo C. Chitosan-based hydrogel to support the paracrine activity of mesenchymal stem cells in spinal cord injury treatment. Sci Rep. 2019;9:6402. https://doi.org/10.1038/s41598-019-42848-w
19. Khanmohammadi M, Sakai S, Taya M. Characterization of encapsulated cells within hyaluronic acid and alginate microcapsules produced via horseradish peroxidase-catalyzed crosslinking. J Biomater Sci Polym Ed. 2019;30(4):295-307. https://doi.org/10.1080/09205063.2018.1562637
20. Zhao L, Weir MD, Xu HH. An injectable calcium phosphate-alginate hydrogel-umbilical cord mesenchymal stem cell paste for bone tissue engineering. Biomaterials. 2010;31(25):6502-6510. https://doi.org/10.1016/j.biomaterials.2010.05.017
21. Araszkiewicz AM, Oliveira EP, Svendsen T, et al. Manganese-labeled alginate hydrogels for image-guided cell transplantation. Int J Mol Sci. 2022;23(5):2465. https://doi.org/10.3390/ijms23052465
22. Zhang W, Liu C, Li F, Song Y, Wang S. Chitosan-based multifunctional biomaterials for spinal cord injury repair: from design to application. Carbohydr Polym. 2023;304:120585.
23. Jafarimanesh MA, Ai J, Shojaei S, Khonakdar HA, Darbemamieh G, Shirian S. Sustained release of valproic acid loaded on chitosan nanoparticles within hybrid of alginate/chitosan hydrogel with/without stem cells in regeneration of spinal cord injury. Prog Biomater. 2023;12(2):87-98. https://doi.org/10.1007/s40204-023-00218-w
24. Jarrah R, Sammak SE, Onyedimma C, Ghaith AK, Moinuddin FM, Bhandarkar AR, et al. The Role of Alginate Hydrogels as a Potential Treatment Modality for Spinal Cord Injury: A Comprehensive Review of the Literature. Neurospine. 2022;19(2):272-280. https://doi.org/10.14245/ns.2244186.093
25. Zhu L, Li R, Jiao S, Wei J, Yan Y, Wang Z, et al. Blood-Brain Barrier Permeable Chitosan Oligosaccharides Interfere with β-Amyloid Aggregation and Alleviate β-Amyloid Protein Mediated Neurotoxicity and Neuroinflammation in a Dose- and Degree of Polymerization-Dependent Manner.

Mar Drugs. 2020;18(10):488. https://doi.org/10.3390/md18100488
26. Li X, Chen J, Xu T, Zhang R, Qian Y. Chitosan-based scaffolds for neural tissue regeneration: recent developments and future perspectives. Bioact Mater. 2024;28:107-128.
27. Zhu L, Liu T, Cai J, Ma J, Chen AM. Repair and regeneration of lumbosacral nerve defects in rats with chitosan conduits containing bone marrow mesenchymal stem cells. Injury. 2015;46(11):2156-2163. https://doi.org/10.1016/j.injury.2015.08.035
28. Mosahebi A, Wiberg M, Terenghi G, Kellerth JO, Novikov LN. Alginate hydrogel and matrigel as potential cell carriers for neurotransplantation. J Biomed Mater Res A. 2006;77(2):242-252. https://doi.org/10.1002/jbm.a.30603
29. Nichol RH, Catlett TS, Onesto MM, Hollender D, Gómez TM. Environmental Elasticity Regulates Cell-type Specific RHOA Signaling and Neuritogenesis of Human Neurons. Stem Cell Reports. 2019;13(6):1006-1021. https://doi.org/10.1016/j.stemcr.2019.10.008
30. Xu B, Yin M, Yang Y, Zou Y, Liu W, Qiao L, et al. Transplantation of neural stem progenitor cells from different sources for severe spinal cord injury repair in rat. Bioact Mater. 2022;23:300-313. https://doi.org/10.1016/j.bioactmat.2022.11.008

CC BY